



www.acsaem.org Article

Effective Lithium Passivation through Graphite Coating for Lithium Metal Batteries

Felix M. Weber, Karl Martin Graff, Ina Kohlhaas, and Egbert Figgemeier*



Cite This: ACS Appl. Energy Mater. 2023, 6, 3413-3421



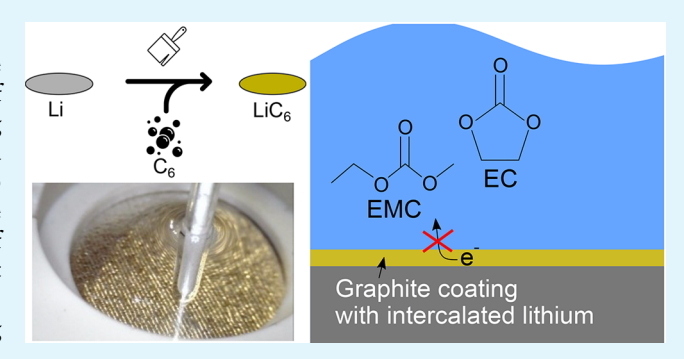
ACCESS

III Metrics & More

Article Recommendations

Supporting Information

ABSTRACT: Metallic lithium reacts with organic solvents, resulting in their decomposition. The prevention of these decomposition reactions is a key aspect enabling the use of metallic lithium as an anode in lithium metal batteries. Scanning electrochemical microscopy (SECM), laser microscopy, and Fourier transform infrared (FT-IR) spectroscopy were used to analyze the effect of a graphite coating on metallic lithium. The graphite layer successfully prevents the agglomeration of decomposition products on the surface. SECM data show that the surface of untreated lithium metal in electrolyte is insulating, but the surface of the graphite coated lithium appears conducting and is therefore not covered by any layer of decomposition



products. The protective properties of the graphite layer were proofed using FT-IR data. No significant differences in the spectra evolved during immersion of the sample in the electrolyte. Electrochemical plating experiments and post-mortem analysis revealed that the graphite layer did not result in homogeneous lithium plating depending on the current density. At high currents, no fully covering layer of decomposition products was formed on the surface during plating experiments, indicating a more complex mechanism of solid—electrolyte interface formation.

KEYWORDS: lithium metal, interphase, hybrid electrode, artificial SEI, SECM

1. INTRODUCTION

Graphite-based anodes are state-of-the-art materials for lithium-ion batteries (LIBs). The theoretical capacity of graphite is 372 mAh/g, while in practical applications the capacity is further limited to 350 mAh/g.^{2,3} A promising material for replacing graphite as anode material is metallic lithium. It has a high theoretical specific energy of 3860 mAh/ g³ but reacts with organic electrolytes, leading to the formation of degradation products.4 In contrast to LIBs, the decomposition products in lithium metal batteries (LMB) do not form an effective passivating layer on the lithium, leading to a continuous decomposition of the electrolyte as well as consumption of metallic lithium (active mass)⁵ and related calendaric aging. Still, these decomposition products agglomerate on the lithium surface and form a nonuniform native solid-electrolyte interface (SEI).⁶ During cycling of the batteries, the repeated plating and stripping of metallic lithium further increases the amount of consumed electrolyte, as the decomposition reaction takes place at the newly created lithium surface. Efficient cycling of lithium-metal anodes is only possible when the lithium plating is controlled at the lithium/electrolyte interface. Thus, multiple suggestions on strategies to enable homogeneous lithium plating have been suggested and discussed.8

Many research groups have focused on the stabilization of the lithium surface to suppress the formation of dendrites during cycling and to improve cycling performance. Several different approaches are used to inhibit dendrite growth.9 Besides the use of hybrid electrolytes, 10-12 concepts for liquid electrolyte-based LMBs are proposed. Liang et al. have successfully suppressed the formation of dendrites and the related formation of a highly resistive layer by melt infusion of lithium into three-dimensional scaffolds, 13 but the production of the electrodes is a complex and time-consuming process. Other groups have treated metallic lithium foil and created a functional layer on top of the lithium surface. Magneton sputtering of amorphous $\text{Li}_3\text{PO}_4^{\ 14}$ or sputtering of $\text{Al}_2\text{O}_3^{\ 15}$ onto metallic lithium led to a more stable cycling performance of LMBs. Promising results were achieved by using hollow carbon nanospheres on metallic lithium. 16 This monolayer successfully prevented the formation of dendrites and allowed cycling for 150 cycles. The production of this covering material

Received: December 23, 2022 Accepted: March 2, 2023 Published: March 17, 2023





is complex and time-consuming. Simpler production of a covering layer was achieved by Zhang et al. They have proposed to protect the lithium metal surface with amorphous carbon through sputtering. Products from electrolyte decomposition on the lithium/carbon surface were still discovered after 50 cycles and assigned to effects of the cycling of the cells. The covering of lithium with graphite has also gained attention from industry in the past years. It is known from literature that carbon nanotubes and lithium can form an LiC_6 interphase on metallic that is highly lithiophilic and may decrease the plating overpotential in batteries. Still, the effect of any covering material on the native SEI on lithium has not yet been studied.

Scanning electrochemical microscopy (SECM) has been successfully used in the past for analysis of the covering layer on metallic lithium. 20-22 SECM is a microscopic method that uses platinum electrodes in the micrometer range. The method can be used to determine the electrochemical activity of any substrate.^{23–25} For using the microscope in the so-called "feedback mode", a redox mediator is added to the electrolyte. Through the application of a constant potential between the microelectrode and the counter electrode, a current is induced. The measured current depends on the distance between the micro electrode and the substrate as well as the electrochemical activity of the substrate. The approach of a conducting substrate with the micro electrode results in an increasing current, whereas the approach to an insulating surface results in a decreasing current. The interested reader may receive extended information on the working principle of the used microscopy in other literature.²⁶ The recorded current during the approach of the microelectrode toward the sample results in an "approach curve" that depends on several parameters as will be described.²⁷ The quantification of these parameters is possible by fitting the experimental data to an analytical function proposed by Cornut and Lefrou. This allows the analysis of the parameters including the substratemicro electrode distance, the insulator thickness around the micro electrode, the active area of the micro electrode itself, and the dimensionless substrate kinetics parameter. This dimensionless parameter describes the kinetics of the reduction reaction of the redox mediator at the substrate surface. For lithium metal, this parameter can be used to quantify the passivation of the lithium surface.²² SECM can be used to identify changes of interphases between metallic lithium and electrolyte as we have shown in a previous publication.²² In the same study, we have shown that electrolytes based on EMC and EC do not form a passivation layer, but instead we have observed a continuously growing layer of deposition products. In order to overcome this instable and dynamic interface behavior, we coated lithium metal foil with a layer of graphite by simple mechanical means. The micrometer-scale graphite coating appears to be a highly potent inhibitor of electrolyte decomposition as we reveal by means of monitoring the surface properties by SECM.

Further electrochemical testing and post-mortem analysis were conducted to understand the effect of the graphite coating on the plating behavior in lithium metal batteries.

2. EXPERIMENTAL SECTION

For the investigation of lithium metal surfaces, Li-chips (99.95%, LTS Research, $\emptyset = 15.6$ mm) were used in the experiments. The surface was modified with graphite powder (MagE3, Hitachi). The powder was put on top of the metal surface and was brushed manually with a

toothbrush under mild mechanical pressure. Excess graphite was mechanically removed, and a visibly stable graphite coating remained. The mechanical stability of the graphite cover revealed itself in the course of the electrochemical experiments. Only few loose particles were observed in electrolyte solutions. All lithium and graphite modified electrodes were strictly handled under argon atmosphere (H_2O and O_2 levels <0.1 ppm).

For the optical surface characterization, the lithium chips were analyzed using a laser microscope (VK-9700K 3D-Laserscan-Colorlaser microscope, Keyence) inside an argon filled glovebox. The surface layer was also analyzed by focused ion beam-scanning electron microscopy (FIB-SEM). Sample preparation and imaging were conducted in a FEI Helios NanoLab 460F1. The sample transfer was carried out in argon atmosphere. The sample was covered with a platinum-based surface layer prior to the milling process. Electrochemical surface evaluation was carried out using SECM in feedback mode, probing surface conductivity.

The graphite coated lithium chip was immersed in electrolyte (LP50, BASF, 1 M LiPF₆ in EC/EMC 1:1 w/w) with 5 mM 1,4-ditert-butyl-2,5-dimethoxybenzene (DBDMB, > 98%, Chemos) as redox mediator. The SECM approach curves were carried out using a SECM setup and platinum micro electrodes with a diameter of 25 μ m from Sensolytics (Bochum, Germany). A platinum coil acted as counter electrode (Sensolytics) and a lithium made from lithium foil (battery grade, 300 µm thickness, Albemarle) as reference electrode. The micro electrode was prepared by polishing it on alumina sandpaper with varying grit sizes (5, 1, and 0.3 μ m) and with silicon oxide (0.03 μ m) on a cloth. The SECM approach curves were measured inside an argon filled glovebox (H2O and O2 levels <0.1 ppm) with an applied potential of 4.10-4.15 V vs Li/Li+, provided by a bipotentiostat (PGSTAT30 with ECD module, Metrohm Autolab). The tip was moved at a speed of 2 μ m/s, a traveled distance of 0.1 μ m, and a waiting time of 15 ms before the current was measured. For controlling the SECM experiment and collecting data, the Sensolytics SECM software was used with an enabled Sallen-Key filter with a RCtime constant of 5 s.

Further information about the surface was gained from FT-IR experiments. In this experiment, lithium foil (Battery grade, $300~\mu m$ thickness, Albemarle) was used, which was treated with graphite powder as described for the chips above. Graphite coated lithium foil and untreated lithium foil were immersed in electrolyte (LP50, BASF). All samples were prepared in an argon filled glovebox (H_2O and O_2 levels <1 ppm). Samples of the metal were taken with tweezers from the solution. The metal was held for a few seconds to allow excess electrolyte to runoff. For analysis, a Vertex70 (Bruker) that was placed in an argon filled glovebox (H_2O and O_2 levels <1 ppm) was used, and the spectra were recorded with a resolution of 4 cm⁻¹ and 16 scans per sample. To compare the results, spectra of graphite powder with the electrolyte were recorded. Graphite powder was given onto the measurement area, and three drops of electrolyte were added on top. The measurement was done as described above.

The lithium plating behavior was evaluated in coin cells. Symmetric CR2032 coin cells with graphite coated lithium chips and 90 μ L electrolyte (LP50, BASF) were built and charged. Two different experiments were conducted, in both of which a charge of 15 mAh was transferred after an initial 24 h resting step: (1) 0.5 mA/cm² for 15 h or (2) 0.1 mA/cm² for 75 h. The same experiment was repeated with untreated lithium. After the constant current treatment, the cells containing the graphite coated lithium were opened and the cathodic lithium was analyzed using laser microscopy (VK-9710, Keyence) and SECM approach curves recorded at different positions. These experiments were performed in the same manner as described above.

To further analyze the reactivity of graphite coated lithium with electrolyte, another SECM experiment was performed. To allow comparability with already published results, ²² the used lithium in this experiment was graphite coated lithium foil (as described above) immersed in electrolyte (EC:EMC 3:7 w/w with 1.2 M LiPF₆, Tomiyama) with 5 mM ferrocene (99%, Alfa Aesar) as redox mediator. To prevent the evaporation of the electrolyte during 3 h of measurement, it was covered with paraffin oil (Vaseline Oil, pure,

pharma grade, PanReac AppliChem) containing 9.5 mM ferrocene. The addition of ferrocene to the covering oil was necessary to suppress any liquid–liquid extraction of ferrocene between the two liquids. The entire setup was placed inside an argon filled glovebox (H_2O and O_2 levels <0.1 ppm).

The SECM approach curves were performed within a two-electrode setup. The used platinum coil counter electrode served additionally as reference electrode. The tip was polarized to 0.340 V, and several approach curves were measured (speed 5 μ m/s in steps of 0.5 μ m, waiting time 20 ms). The approach curve was terminated after the current had changed by 25% compared to the bulk current to prevent piercing of the surface. The tip was then retracted by 400 μ m.

3. RESULTS AND DISCUSSION

The modified lithium surface was visually inspected first. Immediately after the shiny metallic lithium metal surfaces (chips, foils) were treated with graphite powder, a black coating was present. Without the presence of electrolyte, the color of the coating slowly changed from black to a slightly golden appearance within minutes. After the sample was immersed into the electrolyte, the surface became completely golden (see Figure 1). A few graphite particles broke loose.

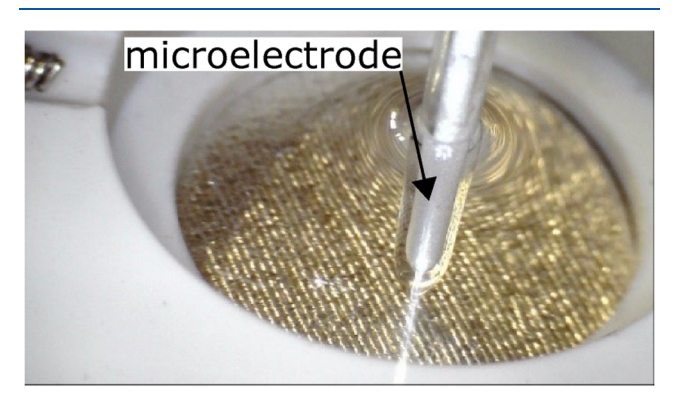


Figure 1. Picture of a graphite coated lithium sample immersed in electrolyte during a SECM measurement.

Still, the entire lithium/graphite surface appeared in golden color. No metallic lithium remained visible at the surface. The golden color indicates that the graphite intercalated lithium as expected. SEM images of cross-sections prove that the entire surface is uniformly covered with the graphite coating (see Figure S1, Supporting Information).

Laser microscopy images of freshly covered lithium samples that were not immersed in electrolyte were recorded for further analysis and evaluation of the cover quality (see Figure 2a). Laser intensity as well as color information are combined in the

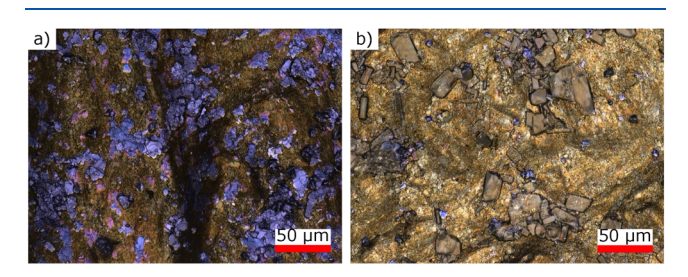


Figure 2. (a) Laser microscope image of the graphite coated lithium prior to immersion in electrolyte and (b) after immersion in the electrolyte for 10 min. Laser intensity and color information are combined in the picture.

image. Here, golden as well as black particles are visible. It is assumed that the golden parts are graphite with intercalated lithium, while the black parts are graphite particles that are inactive with respect to lithium intercalation. 28

The pictures show that the used process is not capable of covering the entire lithium surface with intercalated graphite, but it becomes evident that even without the liquid electrolyte, lithium intercalates in graphite. With the color of the graphite particles turning intensively golden throughout the surface after immersion of the sample into the electrolyte, an efficient intercalation process can be assumed. A laser microscopy image of a sample after immersion into electrolyte is depicted in Figure 2b. Hardly any black particles are visible, indicating a complete intercalation of the used graphite with lithium. It is assumed that the crystals that have formed on the surface are remains from the used electrolyte and could be either EC or conducting salt, as they always appear after immersion of a sample in electrolyte.

The cross-section from FIB-SEM images of the graphite coated lithium is depicted in Figure 3. The bulk lithium is in

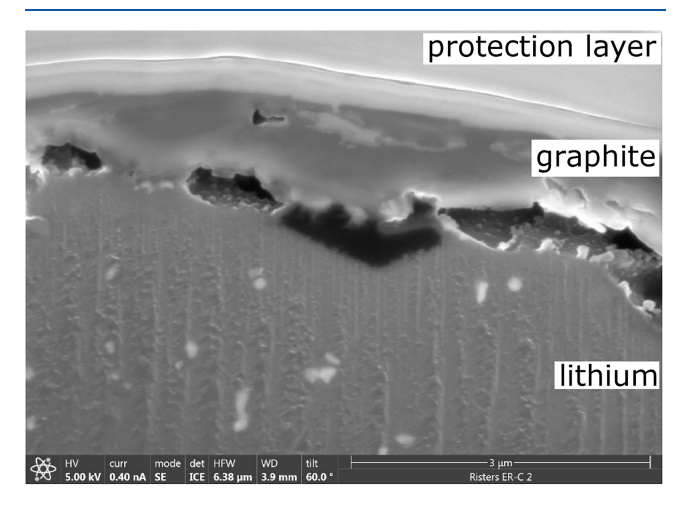
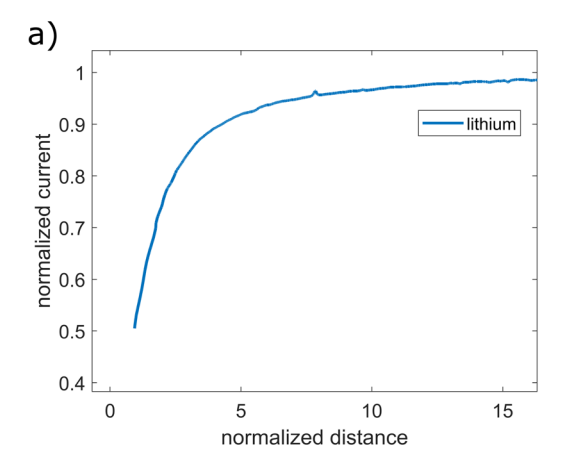


Figure 3. FIB-SEM image of a cut edge of the graphite coated lithium. The very top part above the white line belongs to the protection layer formed for the FIB measurement; the part below the cavities is the lithium. The graphite layer is in between.

the lower part of the picture, while the top surface belongs to the protection layer deposited for the FIB experiments. The graphite layer is between the white line and the cavities. The results indicate that the coating procedure did not produce a thick graphite layer on the surface. Only a thin coating of approximately one micrometer in thickness is observed. The measured thickness varies between 0.9 and 2.8 μ m. The graphite particles are not connected to the bulk lithium over the entire area. Cavities have been formed between the lithium and the graphite coating. With an assumed overall thickness of approximately 1 μ m, a density for graphite of 2.2 g/cm^{3,29} and a theoretical capacity of 372 mAh/g, the graphite layer adds an areal capacity of approximately 8.2 × 10⁻⁵ mAh/cm² and is therefore neglectable in relation to the overall plated amount of lithium.

The surface properties were analyzed using SECM in its feedback mode. The approach curves of the unmodified lithium surface as well as of the graphite coated surface are depicted in Figure 4. The measurement is depicted from right to left, with the surface being at the left side of the graph. The



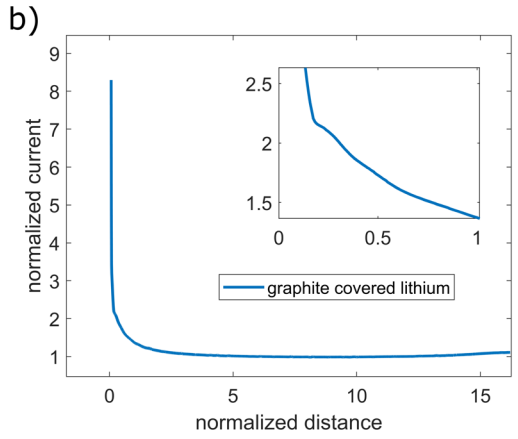


Figure 4. (a) SECM approach curve toward unmodified lithium immersed in electrolyte. (b) SECM approach curve toward graphite coated lithium immersed in electrolyte. The observed corner at a normalized distance of 0.25 is magnified in the inset.

current is normalized by dividing the current with the bulk current of the SECM approach curve, while the distance is normalized by dividing the distance of the tip to the surface with the radius of the tip.

The approach curve toward the unmodified surface shows a decrease of the current in close proximity to the surface. The decreasing current indicates an insulating sample. Metallic lithium reacts with electrolytes without an applied external current. The decomposition products accumulate on the surface and form a native interphase. This passivating layer is electronically insulating and lithium therefore appears as an insulating substrate in SECM experiments.

The approach curve toward the graphite coated lithium surface is depicted in Figure 4b. In contrast to the unmodified lithium surface, the current increases in close proximity to the surface and is therefore a positive feedback. Positive feedback indicates a conducting sample. This shows that the coverage of lithium with graphite successfully inhibits the formation of an insulating passivation layer on the surface. This occurs even though the golden color indicates lithiated graphite and therefore a potential as low as 0.1 V vs Li/Li⁺. At a normalized distance of 0.25, a corner in the graph is observed with a steep increase of the current (see Figure 4b inset). This might be caused by the tip touching the surface, and this causes a very high measured conductivity. The data points prior to touching the surface form an approach curve whose curvature indicates high conductivity. But, the method does not seem to be accurate enough for quantifying how the graphite conductivity is influenced through the intercalation of lithium.

The formation of a passivating surface layer (the SEI) is expected to occur when the anode reaches a potential that is outside of the stability window of the electrolyte. For EC the reduction occurs below 1.36 V (vs Li/Li⁺).³⁰ Both analyzed electrodes, the metallic lithium and the graphite covered lithium are well below this value. Atomic force microscopy (AFM) experiments carried out in EC:DEC-based electrolyte indicate that the SEI changes the most below 0.8 V (vs Li/Li⁺).³¹ Although the golden color of the graphite in our experiment indicates a fully lithiated graphite with the according low voltage of 0.1 V vs lithium, no insulating layer made of decomposition products was electrochemically detected on the surface. It is to be denoted that the surface area of the graphite coated lithium (see Figure S1, Supporting Information) is higher compared to pure metallic lithium. Still,

this higher surface area did not result in an increased electrolyte decomposition and increased formation of an insulating surface layer on top of the electrode surface but inhibited the formation of such a layer of decomposition products according to our results.

Our results show that the surface potential cannot be the only cause for the formation of a passivating surface layer, but other aspects play an important role in the SEI formation. Obviously, the overpotential for the electrolyte reductive decomposition is highly dependent on the material in question.

The changes in the surface properties of the graphite coated lithium were monitored for several hours with repeated SECM approach curves. Within 160 min, the approach curves did not switch to a negative feedback but remained positive, thus indicating the absence of an insulating layer of decomposition products on the surface. The recorded approach curves were fitted to the equation of Cornut and Lefrou¹ to quantify changes in the sample height. As shown in our previous contribution, the passivation layer on metallic lithium grows to more than 1 mm thickness within 3 h when monitored with the same setup in the identical electrolyte.²² The change of the layer height on the graphite coated lithium is depicted in Figure 5.

The resulting layer height of the graphite covered lithium increases during the 160 min by approximately 120 $\mu \rm m$, being equal to a reduction by 99% compared to a nontreated lithium metal sample. The growth seems to saturate with increasing time. The reason for this growth remains unclear at this point. Since the surface of the sample remains conducting, the growth of an insulating surface layer cannot explain this behavior and is therefore ruled out.

From the fit of an approach curve, the dimensionless substrate kinetics parameter κ can be derived. This parameter describes the kinetics of the reduction of the redox mediator at the sample and is dependent on the active area of the micro electrode a, the kinetic reaction constant of the mediator at the substrate k, and the diffusion coefficient D:

$$\kappa = \frac{ka}{D} \tag{1}$$

This parameter was monitored for graphite coated lithium during the immersion in electrolyte. Its value changes by less than $10^{-8}\%$ over 160 min, indicating that the kinetics of the mediator reaction remained approximately constant. We

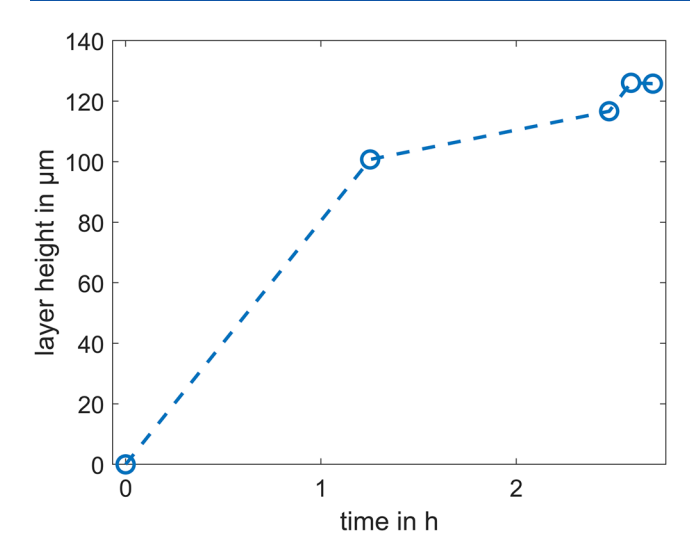


Figure 5. Difference of the surface position of SECM experiments on graphite coated lithium, which is immersed in electrolyte. The surface position was calculated according to the equation by Cornut and Lefrou. The dashed lines are only a guide to the eye.

conclude that no passivating layer has formed on the surface during this period of time and a steady-state situation is reached. The reason for an increasing layer height with remaining positive feedback remains unclear, but several mechanisms are possible.

Although the graphite coating appears to cover the entire surface, lithium metal is likely to be still in direct contact with the electrolyte at defects in the coating. Therefore, lithium, which is exposed to the electrolyte, could react and form decomposition products that agglomerate on the surface as shown for metallic lithium.²² Furthermore, the graphite might take up the electrolyte and swell. Both mechanisms might add to the total layer height. Since the SECM approach curves still show a positive feedback after 160 min, the development of an insulating passivation layer on the surface due to agglomeration of decomposition products appears neglectable. Still, decomposition products may form and build up underneath the graphite layer, thus elevating this graphite layer. A final conclusion on the observations cannot be drawn at this point and will be a matter for further studies.

To further analyze changes on the surface during immersion of the sample in electrolyte, FT-IR spectra were recorded (see Figure 6). During immersion of the noncoated lithium for 18 h, changes in the spectra at different wavelengths were observed. The identification of exact vibrations and related decomposition products was not carried out. The measurements show that no stable and inert surface was built on the lithium. In contrast, on the graphite coated lithium in the electrolyte, no significant changes in the absorption bandwidths between 400 and 4000 cm⁻¹ could be observed. Slight changes in the intensities are attributed to the sample preparation and different amounts of remaining electrolyte on the surface. For detailed analysis of IR data of electrolytes, the interested reader may refer to literature as this discussion is outside of the scope of this manuscript.³² For comparison, a spectrum of graphite powder soaked with electrolyte was recorded. The spectrum of graphite powder with electrolyte has the same absorption bandwidths, except for one missing signal at 660 cm⁻¹. The signal at 660 cm⁻¹ (pink square) is assigned to intercalated lithium in the graphite.³³ This is likely

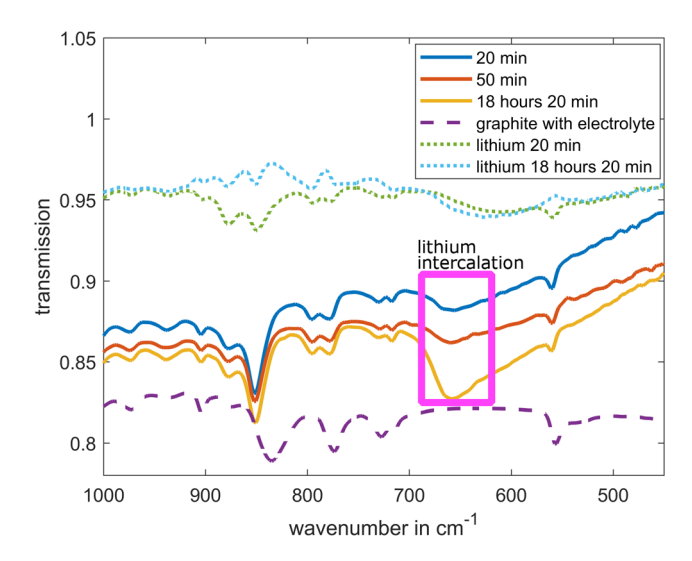


Figure 6. FT-IR spectra of graphite coated lithium foil (solid lines) and noncoated lithium foil (dotted lines) after immersion in EC:EMC-based electrolyte for different times. The dashed line represents the reference measurement of graphite powder with electrolyte. This spectrum was compressed by a factor of 0.1 and shifted to higher transmission values to allow comparison with the other data.

since the golden color indicates the presence of lithium that is intercalated into graphite. Longer immersion of the carbon treated lithium leads to an increased signal intensity at $660 \, \mathrm{cm}^{-1}$. This allows to follow the intercalation of lithium into graphite in situ.

Since the rest of the spectrum does not change over time and all peaks can be assigned either to the pure electrolyte or intercalation compounds, we assume that no significant changes on the surface occur. This supports the results from the SECM experiments that no significant surface layer is formed by a purely chemical reaction between the sample and the electrolyte.

Further studies were carried out to analyze the effect of cycling batteries with the modified lithium. Symmetrical CR2032 coin cells were used to evaluate the plating behavior of the graphite coated lithium. A total of 8 mAh/cm 2 was plated onto the graphite coated lithium with either 0.5 or 0.1 mA/cm 2 .

The resulting potential curve during the plating process of the graphite coated lithium with 0.1 mA/cm² is depicted in Figure 7 (red line). At the beginning of the plating process, an overpotential of 17 mV was measured. This decreases to 11 mV and remains constant throughout the plating process. For comparison, the same experiment was repeated with untreated metallic lithium (see Figure 7, blue line). Initially, an overpotential of 27 mV was measured, which was quickly reduced to 16 mV and further reduced to 13 mV during the entire plating process. When the metallic lithium is treated by brushing over the surface in order to fully separate the effect of surface treatment and the graphite layer (see Figure 7, yellow line), it becomes evident that all effects that were previously described can be assigned to the graphite layer itself and that the mechanical treatment of the surface does not have any significant effect toward a decrease of the overpotential. It is expected that the removal of the surface layer enables fresh reactive lithium to react with the electrolyte in order to form a more resistive surface layer than it was present before the

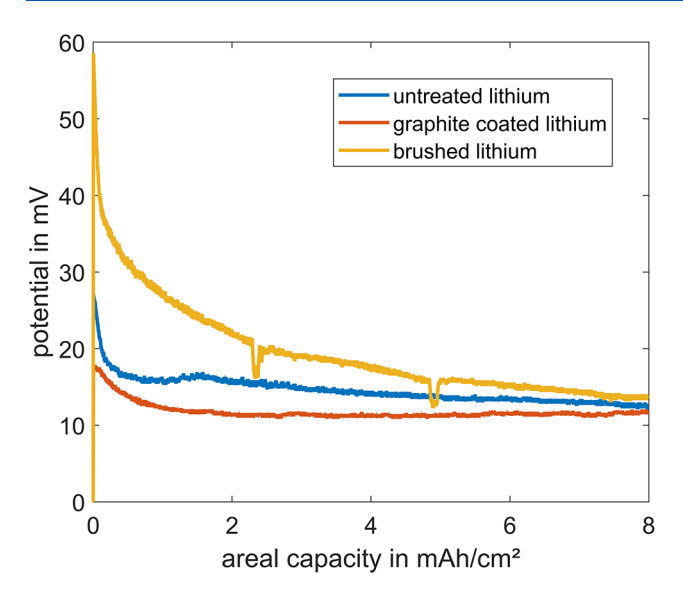


Figure 7. Voltage profile of symmetrical coin cells with either untreated lithium, graphite coated lithium or brushed lithium during plating with 0.1 mA/cm².

abrasive treatment, which then results in an increased overpotential. The fluctuations occurring in the potential of the brushed lithium are occurring in all built cells, and it is therefore questioned that they are related to measurement errors. Still, the origin of these fluctuations remains unclear at this point.

The initial overpotential during plating and stripping of a symmetrical lithium metal battery is attributed to a kinetic hindrance by a surface film toward the deposition of lithium ions³⁴ or hindrance in the nucleation step itself.³⁵ A possible hindrance of the nucleation step is questioned since it cannot explain the increase of the overvoltage in symmetrical coin cells in the second and higher cycles, as will be discussed later.

Concerning the assumption of breaking layers, the deposition of lithium ions leads to the breakage of the film and a reduced overpotential after the initial maximum.³⁴ A lower initial overpotential therefore can be assigned to a thinner surface layer. This supports the previous results that the graphite layer successfully prevents the formation of a thick deposition layer on top of the lithium.

The decrease of the overpotential after the initial maximum when using untreated lithium indicates a continuously changing surface and a further decrease of the kinetic hindrance toward lithium plating through breaking of the surface layer. Still, even after plating 8 mAh/cm² in 75 h, the overpotential is higher than the one measured with graphite coated lithium. The overpotential of the coin cell with graphite coated lithium remains constant after the initial maximum. This indicates that no further breaking of a surface layer occurs. It is concluded that, in accordance with the already described results, the graphite coating prevents the formation of a passivating surface layer and enables lithium deposition with a lower kinetic hindrance than observed on untreated lithium.

When using higher currents in the plating experiments, the overpotential at the beginning of the plating is higher for untreated and graphite coated lithium (see Figure 8) compared to the described experiments at lower current. The untreated lithium has an initial overpotential of approximately 500 mV when plating with a current of 2.5 mA/cm². After plating 0.5

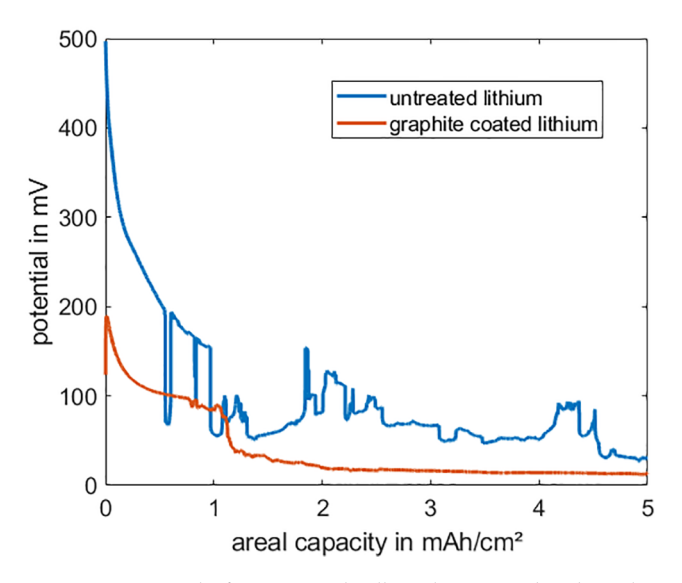


Figure 8. Potential of symmetrical cells with untreated and graphite coated lithium during initial plating with 2.5 mA/cm².

mAh/cm², the current starts to fluctuate. This behavior is reproducible over all tested cells. It is likely that the higher currents used lead to the formation of dendrites on the lithium, resulting in short circuits. The formation of locally higher amounts of lithium after plating in symmetrical lithium-metal cells that may lead to the formation of dendrites is known from literature.³⁶ The overpotential of the graphite coated lithium is approximately 200 mV and therefore lower compared to the untreated lithium. This proves that the reduced overpotential for graphite coated lithium and all assumptions made remain valid for higher plating currents. Still, these cells have a voltage drop after plating 1 mAh/cm² onto the lithium. It is assumed that this is again caused by dendrites that form on the graphite coated lithium and result in short circuits. As a result, the developed coating method is capable of minimizing the electrolyte decomposition reaction but may not inhibit the growth of dendrites at high currents. Detailed evaluation of the plating behavior of the graphite coated cells will therefore only be performed on the cells with a plating current of 0.1 and 0.5 mAh/cm^2 .

During consecutive cycling with 0.1 mAh/cm² overpotential of both samples, the graphite coated lithium as well as the untreated lithium decreases compared to the first plating process. The differences in the voltage curves of both samples decrease as well (see Figure 9). This indicates that the effect of the graphite coating decreases as the cycle number increases. In the second and higher plating steps, a difference in the potential curve in contrast to the first plating is observable. Toward the end of the plating process, the overpotential increases again.

In literature, two different explanations for the overpotential during plating and stripping are suggested. The first assumes that the overpotentials only originate from the hindrance of the nucleation step itself,³⁵ but this assumption cannot explain the increase of the potential toward the end of the plating step. Therefore, the validity of this model might be questioned. The second model of braking layers³⁴ assumes that the overpotential increases because the freshly plated lithium from the last plating step is used up and the bulk lithium is harder to strip from because of a more stable surface layer, resulting in a higher overpotential. Due to the fast decrease of the effect, the

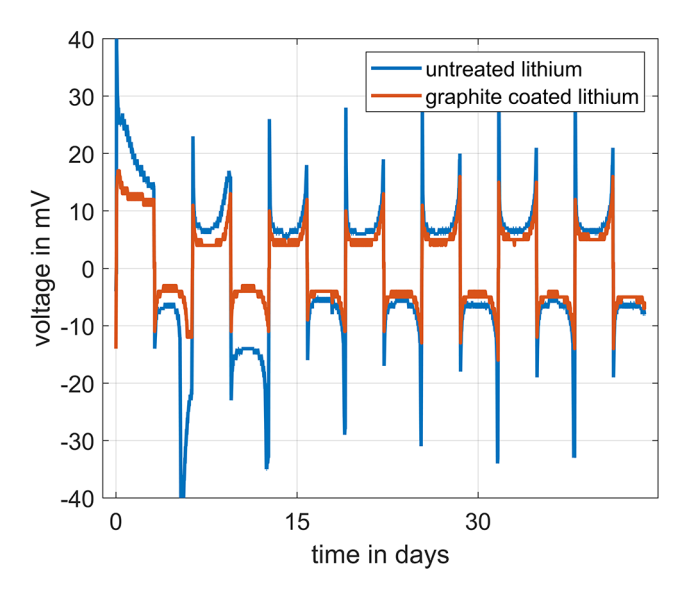


Figure 9. Voltage over time of symmetrical coin cells with either graphite coated lithium or untreated lithium.

changes of the graphite coating were analyzed after the first plating.

The cathodic graphite coated lithium from the plating experiments was evaluated post-mortem using SECM and laser microscopy. Images from the laser microscope are depicted in Figure 10, where laser intensity and color information are combined.

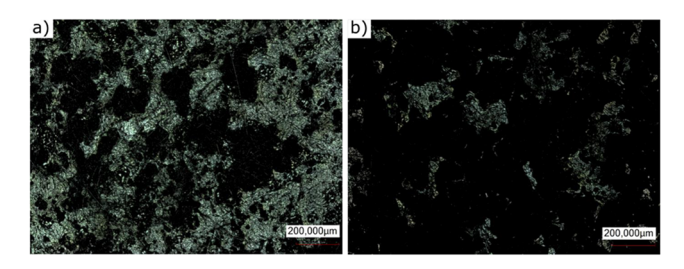


Figure 10. Laser microscope images of graphite coated lithium after plating of 8 mAh/cm². Laser intensity and color information are combined: (a) with a current density of 0.5 mA/cm², (b) with a current density of 0.1 mA/cm².

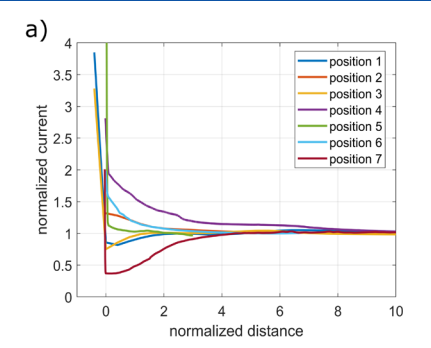
On the lithium that was plated with 0.5 mA/cm² (see Figure 10a), a coverage of the surface with a silver/metallic structure is visible, but no homogeneous plating has occurred. Still, some

black parts are visible that can be assigned to the graphite particles. Although the sample still appeared golden after removal from the coin cell, the golden color cannot be observed in the microscope images. The present metallic structure on the surface is plated lithium. In contrast, the lithium/graphite surface of the coin cell that was plated on with 0.1 mA/cm² looks mostly black (see Figure 10b). Only some metallic areas are visible, while the amount of transferred charge is identical in both coin cells. It may be assumed that high currents lead to a larger share of lithium coverage than smaller currents as already reported in literature. 37,38 The amount of plated lithium appears to be smaller in the cell with the low current density. Although our FT-IR experiments indicate that the graphite is not fully intercalated, we doubt the possibility that large quantities of the plated lithium may have intercalated into the graphite since the assumed capacity of the graphite is neglectable as calculated above. Since the golden color indicates an at least partially intercalated graphite before charging the cells with a total of 8 mAh/cm², further intercalation of large quantities of the plated lithium is unlikely. Plating of lithium underneath the graphite layer, as well as reactions of the plated lithium with the electrolyte, might occur. The plating of lithium underneath a carbon layer in a similar setup was already described in literature. 16 It is assumed that this also occurs in the present system. The lithium ions might intercalate into the graphite and be reduced to metallic lithium at the graphite/lithium interface. The observed metallic lithium on top of the graphite in Figure 10 may originate from a diffusion limitation of lithium ions in the graphite. As a result, the graphite cannot accommodate any more lithium ions, resulting in lithium plating on the surface.

To gain further knowledge about the ongoing processes during lithium plating SECM approach, curves were recorded at different positions after the plating experiment (see Figure 11).

The current was normalized to the current in the bulk regime, and the distance was normalized by dividing the distance from the surface through the tip radius. The position of the surface was approximated from the approach curve data and is not accurate.

Figure 11a depicts the approach curves for the electrode that was plated on with 0.5 mA/cm². Approach curves with positive and negative feedback are present. All approach curves show a steep increase at the 0 tick. This is attributed to the tip touching the sample and piercing the surface. Underneath a layer of decomposition products that might be present, and underneath the graphite layer, a metallic surface is present.



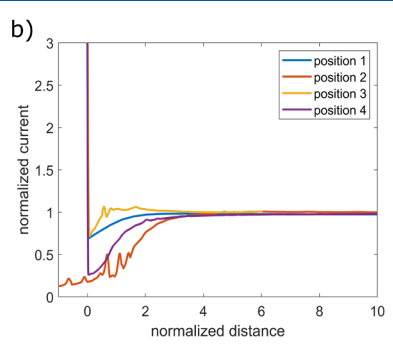


Figure 11. SECM approach curves of graphite coated lithium after plating of 8 mAh/cm²: (a) with a current density of 0.5 mA/cm², (b) with a current density of 0.1 mA/cm².

Piercing through these layers results in physical contact of the microelectrode and the metal, meaning a short circuit and very high current. The presence of negative feedback curves indicates that in some areas on the electrode a decomposition layer has formed. Still, some positive feedback curves are recorded, indicating that not the entire electrode is coated with a decomposition layer. The feedback curves are not completely positive or completely negative but differ in their feedback intensity. This shows that the surface is not uniform but differs in quality throughout the surface.

On the graphite coated electrode that was plated with 0.1 mA/cm², only negative feedback curves are recorded. Some of the approach curves are not smooth, but rough, which may arise from noise due to the small currents. The present negative feedback curves show that the electrode appears to be fully coated with a decomposition layer regarding the resolution that can be achieved with our setup. Similar to the results from the electrode that was plated with a higher current, the approach curves differ in the intensity of the feedback. Therefore, the decomposition layer is not uniform.

With the layer covering the entire surface and the laser microscopy images showing less plated lithium, parts of the plated lithium may have reacted with the electrolyte. As it is already known from literature, lithium reacts with electrolyte, forming thick decomposition layers.²² It is concluded that the used graphite covering efficiently suppresses the reactions of metallic lithium with the electrolyte but cannot lead to a fully reversible plating for all current densities as it does not suppress the reactions of the on-top plated lithium with the electrolyte.

4. CONCLUSIONS

The effect of a graphite coating on lithium metal with respect to electrolyte decomposition and plating effects was studied. Brushing graphite powder onto the surface is a simple technique to cover lithium metal. The graphite coating effectively protects the electrolyte from being decomposed at the lithium surface. Our studies show that the formation of a SEI layer not only depends on the electrochemical potential of a sample. The lithiated graphite has a potential outside the stability window of the electrolyte, but no surface layer was formed after immersion in electrolyte. The graphite cover efficiently prevented the decomposition of the electrolyte within several hours, which was proven using SECM and FT-IR data. SECM data showed that within 2.5 h, a shift in the surface position by 120 μ m had occurred, which might originate from graphite swelling. The SECM data additionally showed that the forming layer is not electrically insulating and, therefore, cannot serve as SEI layer.

Further plating tests revealed that high plating currents led to a thicker film of metallic lithium on the surface of graphite coated lithium. In contrast, on the graphite coated lithium sample that was plated with a low current of $0.1~\text{mA/cm}^2$, almost no metallic layer was visible. SECM studies of these samples showed that plating with a low current leads to a surface that is fully covered with an insulating surface layer. High currents of $0.5~\text{mA/cm}^2$ result in a surface that is partially insulating and partially conducting. It is assumed that the insulating surface layer originates from reactions of the lithium with the electrolyte.

It is concluded that covering lithium with graphite is an effective tool to prevent the decomposition of electrolyte on the surface. Though plating characteristics seem to be

significantly improved at low current densities, plating homogeneity suffers with higher current densities.

ASSOCIATED CONTENT

Supporting Information

The Supporting Information is available free of charge at https://pubs.acs.org/doi/10.1021/acsaem.2c04128.

Cross-section SEM image of graphite coating lithium (PDF)

AUTHOR INFORMATION

Corresponding Author

Egbert Figgemeier – Helmholtz Institute Münster (HI MS), IEK-12, Forschungszentrum Jülich GmbH, 52074 Aachen, Germany; Institute for Power Electronics and Electrical Drives (ISEA), RWTH Aachen University, 52074 Aachen, Germany; JARA-Energy, 52425 Jülich, Germany; Email: e.figgemeier@fz-juelich.de

Authors

Felix M. Weber — Helmholtz Institute Münster (HI MS), IEK-12, Forschungszentrum Jülich GmbH, 52074 Aachen, Germany; orcid.org/0000-0002-1641-6620

Karl Martin Graff – Institute for Power Electronics and Electrical Drives (ISEA), RWTH Aachen University, 52074 Aachen, Germany

Ina Kohlhaas – Institute for Power Electronics and Electrical Drives (ISEA), RWTH Aachen University, 52074 Aachen, Germany

Complete contact information is available at: https://pubs.acs.org/10.1021/acsaem.2c04128

Notes

The authors declare no competing financial interest.

ACKNOWLEDGMENTS

The authors would like to thank Lea Risters from the Ernst Ruska-Centre for Microscopy and Spectroscopy with Electrons for making the FIB-SEM imaging. This work was conducted as part of the US-German joint collaboration on "Interfaces and Interphases in Rechargeable Li-metal based Batteries" supported by the US Department of Energy (DOE) and German Federal Ministry of Education and Research (BMBF). Financial support was provided by the German Federal Ministry of Education and Research (BMBF), Grant No. 13XP0225B.

REFERENCES

- (1) Cornut, R.; Lefrou, C. New analytical approximation of feedback approach curves with a microdisk SECM tip and irreversible kinetic reaction at the substrate. *J. Electroanal. Chem.* **2008**, *621* (2), 178–184
- (2) Tarascon, J. M.; Armand, M. Issues and challenges facing rechargeable lithium batteries. *Nature* **2001**, *414* (6861), 359–367.
- (3) Zhang, J.-G.; Xu, W.; Henderson, W. A. Lithium Metal Anodes and Rechargeable Lithium Metal Batteries. MRS Bull. 2017, 42, 857.
- (4) Peled, E. The Electrochemical Behavior of Alkali and Alkaline Earth Metals in Nonaqueous Battery Systems—The Solid Electrolyte Interphase Model. *J. Electrochem. Soc.* **1979**, *126* (12), 2047–2047.
- (5) Wood, S. M.; Fang, C.; Dufek, E. J.; Nagpure, S. C.; Sazhin, S. V.; Liaw, B.; Meng, Y. S. Predicting Calendar Aging in Lithium Metal Secondary Batteries: The Impacts of Solid Electrolyte Interphase Composition and Stability. *Adv. Energy Mater.* **2018**, 8 (26), 1801427.

- (6) Deng, K.; Han, D.; Ren, S.; Wang, S.; Xiao, M.; Meng, Y. Singleion conducting artificial solid electrolyte interphase layers for dendrite-free and highly stable lithium metal anodes. *Journal of Materials Chemistry A* **2019**, 7 (21), 13113–13119.
- (7) Lee, H.; Lee, D. J.; Kim, Y. J.; Park, J. K.; Kim, H. T. A simple composite protective layer coating that enhances the cycling stability of lithium metal batteries. *J. Power Sources* **2015**, 284, 103–108.
- (8) Cao, W.; Li, Q.; Yu, X.; Li, H. Controlling Li deposition below the interface. eScience 2022, 2 (1), 47–78.
- (9) Zhang, X.; Sun, C. Recent advances in dendrite-free lithium metal anodes for high-performance batteries. *Phys. Chem. Chem. Phys.* **2022**, 24 (34), 19996–20011.
- (10) Qiu, G.; Lu, L.; Lu, Y.; Sun, C. Effects of Pulse Charging by Triboelectric Nanogenerators on the Performance of Solid-State Lithium Metal Batteries. ACS Appl. Mater. Interfaces 2020, 12 (25), 28345–28350.
- (11) Yi, Q.; Zhang, W.; Wang, T.; Han, J.; Sun, C. A High-performance Lithium Metal Battery with a Multilayer Hybrid Electrolyte. *Energy & Environmental Materials* **2023**, *6* (1), No. e12289.
- (12) Liu, Y.; Li, Y.; Chen, L.; Yan, F.; Lin, Z.; Wang, J.; Qiu, J.; Cao, G.; Wang, B.; Zhang, H. Expanding the reversibility of graphite-Li metal hybrid anodes by interface and inner-structure modifications. *Energy Storage Materials* **2022**, *53*, 621–628.
- (13) Liang, Z.; Lin, D.; Zhao, J.; Lu, Z.; Liu, Y.; Liu, C.; Lu, Y.; Wang, H.; Yan, K.; Tao, X.; Cui, Y. Composite lithium metal anode by melt infusion of lithium into a 3D conducting scaffold with lithiophilic coating. *Proc. Natl. Acad. Sci. U.S.A.* **2016**, *113* (11), 2862–2867.
- (14) Wang, L.; Wang, Q.; Jia, W.; Chen, S.; Gao, P.; Li, J. Li metal coated with amorphous Li3PO4via magnetron sputtering for stable and long-cycle life lithium metal batteries. *J. Power Sources* **2017**, 342, 175–182.
- (15) Wang, L.; Zhang, L.; Wang, Q.; Li, W.; Wu, B.; Jia, W.; Wang, Y.; Li, J.; Li, H. Long lifespan lithium metal anodes enabled by Al2O3 sputter coating. *Energy Storage Materials* **2018**, *10*, 16–23.
- (16) Zheng, G.; Lee, S. W.; Liang, Z.; Lee, H. W.; Yan, K.; Yao, H.; Wang, H.; Li, W.; Chu, S.; Cui, Y. Interconnected hollow carbon nanospheres for stable lithium metal anodes. *Nat. Nanotechnol.* **2014**, 9 (8), 618–623.
- (17) Zhang, Y. J.; Liu, X. Y.; Bai, W. Q.; Tang, H.; Shi, S. J.; Wang, X. L.; Gu, C. D.; Tu, J. P. Magnetron sputtering amorphous carbon coatings on metallic lithium: Towards promising anodes for lithium secondary batteries. *J. Power Sources* **2014**, *266*, 43–50.
- (18) Krause, L. J.; Jensen, L. D. Graphite modified lithium metal anode. International Patent Application PCT/US 2016/043291, 2017.
- (19) Shi, P.; Li, T.; Zhang, R.; Shen, X.; Cheng, X. B.; Xu, R.; Huang, J. Q.; Chen, X. R.; Liu, H.; Zhang, Q. Lithiophilic LiC₆ Layers on Carbon Hosts Enabling Stable Li Metal Anode in Working Batteries. *Adv. Mater.* **2019**, *31* (8), 1807131.
- (20) Bülter, H.; Peters, F.; Schwenzel, J.; Wittstock, G. Investigation of electron transfer properties of the SEI on metallic lithium electrodes by SECM at open circuit. ECS Trans. 2015, 66 (9), 69–79.
- (21) Bülter, H.; Peters, F.; Schwenzel, J.; Wittstock, G. Comparison of Electron Transfer Properties of the SEI on Graphite Composite and Metallic Lithium Electrodes by SECM at OCP. *J. Electrochem. Soc.* **2015**, *162* (13), A7024–A7036.
- (22) Weber, F. M.; Kohlhaas, I.; Figgemeier, E. Tuning the Reactivity of Electrolyte Solvents on Lithium Metal by Vinylene Carbonate. *J. Electrochem. Soc.* **2020**, *167* (14), 140523.
- (23) Sun, P.; Laforge, F. O.; Mirkin, M. V. Scanning electrochemical microscopy in the 21st century. *Phys. Chem. Chem. Phys.* **2007**, 9 (7), 802–823.
- (24) Wittstock, G.; Burchardt, M.; Pust, S. E.; Shen, Y.; Zhao, C. Scanning electrochemical microscopy for direct imaging of reaction rates. *Angewandte Chemie International Edition* **2007**, 46 (10), 1584–1617.
- (25) Bozic, B.; Figgemeier, E. Scanning electrochemical microscopy under illumination: An elegant tool to directly determine the mobility

- of charge carriers within dye-sensitized nanostructured semiconductors. *Chem. Commun.* **2006**, No. 21, 2268–2270.
- (26) Bard, A. J.; Denuault, G.; Friesner, R. A.; Dornblaser, B. C.; Tuckerman, L. S. Scanning Electrochemical Microscopy: Theory and Application of the Transient (Chronoamperometric) SECM Response. *Anal. Chem.* **1991**, *63* (13), 1282–1288.
- (27) Bard, A. J.; Mirkin, M. V. Scanning Electrochemical Microscopy; CRC Press, 2001.
- (28) Shellikeri, A.; Watson, V.; Adams, D.; Kalu, E. E.; Read, J. A.; Jow, T. R.; Zheng, J. S.; Zheng, J. P. Investigation of Pre-lithiation in Graphite and Hard-Carbon Anodes Using Different Lithium Source Structures. *J. Electrochem. Soc.* 2017, 164 (14), A3914–A3924.
- (29) CRC Handbook of Chemistry and Physics, 89th ed.; CRC Press/Taylor and Francis: Boca Raton, FL, 2009.
- (30) Zhang, X.; Kostecki, R.; Richardson, T. J.; Pugh, J. K.; Ross, P. N. Electrochemical and Infrared Studies of the Reduction of Organic Carbonates. *J. Electrochem. Soc.* **2001**, *148* (12), A1341–A1341.
- (31) Steinhauer, M.; Stich, M.; Kurniawan, M.; Seidlhofer, B. K.; Trapp, M.; Bund, A.; Wagner, N.; Friedrich, K. A. In Situ Studies of Solid Electrolyte Interphase (SEI) Formation on Crystalline Carbon Surfaces by Neutron Reflectometry and Atomic Force Microscopy. *ACS Appl. Mater. Interfaces* **2017**, 9 (41), 35794–35801.
- (32) Saqib, N.; Ganim, C. M.; Shelton, A. E.; Porter, J. M. On the Decomposition of Carbonate-Based Lithium-Ion Battery Electrolytes Studied Using Operando Infrared Spectroscopy. *J. Electrochem. Soc.* **2018**, *165* (16), A4051–A4057.
- (33) Bondarenko, G. N.; Nalimova, V. A.; Fateev, O. V.; Guérard, D.; Semenenko, K. N. Vibrational spectra of superdense lithium graphite intercalation compounds. *Carbon* **1998**, *36* (7–8), 1107–1112
- (34) Bieker, G.; Winter, M.; Bieker, P. Electrochemical in situ investigations of SEI and dendrite formation on the lithium metal anode. *Phys. Chem. Chem. Phys.* **2015**, *17* (14), 8670–8679.
- (35) Horstmann, B.; Shi, J.; Amine, R.; Werres, M.; He, X.; Jia, H.; Hausen, F.; Cekic-Laskovic, I.; Wiemers-Meyer, S.; Lopez, J.; Galvez-Aranda, D.; Baakes, F.; Bresser, D.; Su, C.-C.; Xu, Y.; Xu, W.; Jakes, P.; Eichel, R.-A.; Figgemeier, E.; Krewer, U.; Seminario, J. M.; Balbuena, P. B.; Wang, C.; Passerini, S.; Shao-Horn, Y.; Winter, M.; Amine, K.; Kostecki, R.; Latz, A. Strategies towards enabling lithium metal in batteries: interphases and electrodes. *Energy Environ. Sci.* 2021, 14, 5289–5314.
- (36) Kühnle, H.; Knobbe, E.; Figgemeier, E. In Situ Optical and Electrochemical Investigations of Lithium Depositions as a Function of Current Densities. *J. Electrochem. Soc.* **2022**, *169* (4), 040528–040528.
- (37) Sagane, F.; Ikeda, K. I.; Okita, K.; Sano, H.; Sakaebe, H.; Iriyama, Y. Effects of current densities on the lithium plating morphology at a lithium phosphorus oxynitride glass electrolyte/copper thin film interface. *J. Power Sources* **2013**, 233, 34–42.
- (38) Pei, A.; Zheng, G.; Shi, F.; Li, Y.; Cui, Y. Nanoscale Nucleation and Growth of Electrodeposited Lithium Metal. *Nano Lett.* **2017**, *17* (2), 1132–1139.